Prototyping an ARAIM Offline Ground Monitor Using Experimental Data

Jaymin Patel, *Illinois Institute of Technology*
Yawei Zhai, *Shanghai Jiao Tong University*
Shahriar Kiarash, Samer Khanafseh, *Illinois Institute of Technology*
Mathieu Joerger, *The University of Arizona*
Boris Pervan, *Illinois Institute of Technology*

BIOGRAPHY

Jaymin Patel is a PhD student at Navigation Laboratory in the Department of Mechanical and Aerospace Engineering at IIT. He received his B.S. in Mechatronics Engineering from Ganpat University, Gujarat, India and M.E degree in Mechanical and Aerospace Engineering, from the IIT. His research interests includes the design of high accuracy and high integrity navigation algorithms, fault detection for Ground Based Augmentation Systems (GBAS) and fault monitoring for Advanced Receiver Autonomous Integrity Monitoring (ARAIM). He was the recipient of Best Student Paper Award in the 2018 IEEE/ION PLANS conference.

Dr. Yawei Zhai obtained a Bachelor's degree in Mechanical Engineering from the Qingdao University of Science and Technology, China, in 2013, and a Ph.D. in Mechanical and Aerospace Engineering from the Illinois Institute of Technology (IIT), in 2018. He is currently a post-doctoral researcher at Shanghai Jiao Tong University (SJTU). His research focuses on developing advanced receiver autonomous integrity monitoring (ARAIM) fault detection and exclusion (FDE) methodology to ensure high navigation integrity and continuity for civil aviation using multi-constellation global navigation satellite systems (GNSS).

Shahriar Kiarash received his B.S in Aerospace Engineering in 2018 at IIT. He is expected to complete his M.S in May 2020. He was also dean's student list nominee in 2015 and 2018. He joined the Navigation Lab in 2017 and is passionate about GNSS and navigation field.

Dr. Samer Khanafseh is currently a research assistant professor at Illinois Institute of Technology (IIT), Chicago. He received his MSc and PhD degrees in Aerospace Engineering from IIT in 2003 and 2008, respectively. Dr. Khanafseh has been involved in several aviation applications such as Autonomous Airborne Refueling (AAR) of unmanned air vehicles, autonomous shipboard landing for NUCAS and JPALS programs and Ground Based Augmentation System (GBAS). His research interests are focused on high accuracy and high integrity navigation algorithms, cycle ambiguity resolution, high integrity applications, fault monitoring and robust estimation techniques. He was the recipient of the 2011 Institute of Navigation Early Achievement Award for his outstanding contributions to the integrity of carrier phase navigation systems.

Dr Mathieu Joerger obtained a Diplôme d´Ingénieur in Mechatronics from the Ecole Nationale Supérieure des Arts et Industries de Strasbourg, France, in 2002, and a M.S. and a Ph.D. in Mechanical and Aerospace Engineering from the Illinois Institute of Technology (IIT), in 2002 and 2009 respectively. He is the 2009 recipient of the Institute of Navigation (ION) Parkinson award, and the 2014 recipient of the ION's Early Achievement Award. He is currently an assistant professor at The University of Arizona, working on multi-sensor integration, sequential fault-detection for multi-constellation navigation systems, and relative and differential receiver autonomous integrity monitoring (RAIM).

Dr. Boris Pervan is a Professor of Mechanical and Aerospace Engineering at IIT, where he conducts research on advanced navigation systems. Prior to joining the faculty at IIT, he was a spacecraft mission analyst at Hughes Aircraft Company (now Boeing) and a postdoctoral research associate at Stanford University. Prof. Pervan received his B.S. from the University of Notre Dame, M.S. from the California Institute of Technology, and Ph.D. from Stanford University. He is an Associate Fellow of the AIAA, a Fellow of the Institute of Navigation (ION), and Editor-in-Chief of the ION journal NAVIGATION. He was the recipient of the IIT Sigma Xi Excellence in University Research Award (2011, 2002), Ralph Barnett Mechanical and Aerospace Dept. Outstanding Teaching Award (2009, 2002), Mechanical and Aerospace Dept. Excellence in Research Award

(2007), University Excellence in Teaching Award (2005), IEEE Aerospace and Electronic Systems Society M. Barry Carlton Award (1999), RTCA William E. Jackson Award (1996), Guggenheim Fellowship (Caltech 1987), and Albert J. Zahm Prize in Aeronautics (Notre Dame 1986).

ABSTRACT

This paper describes the prototyping of an offline ground monitor for advanced receiver autonomous integrity monitoring (ARAIM). The ARAIM user algorithm, which includes fault detection and exclusion (FDE), is autonomously executed at the airborne receiver. To achieve specific integrity and continuity requirements, the real-time FDE process requires assertions on the signal-in-space (SIS) performance, in particular on satellite clock and orbit ephemeris error characteristics. This information is broadcast in the integrity support message (ISM). To validate the ISM, the offline ground monitor estimates precise GNSS satellite orbits and clocks which are utilized to validate the ISM. There are many sophisticated orbit determination processes such as the one used by the international GNSS service (IGS), whose performance is specified in terms of accuracy. In contrast, the proposed offline monitor (OFM) architecture is mainly intended for safety-critical aviation applications, in which integrity is of primary concern. This monitor employs a straightforward approach to estimate satellite orbit/clock using the existing satellite based augmentation system (SBAS) ground infrastructure. For prototyping purpose, twenty sparsely-distributed reference stations (RS) are selected from a worldwide network of IGS stations, and their publicly-available observation data is utilized. A parametric satellite orbital model is employed in the estimator, whose implementation is described step by step in the paper. Receiver noise and multipath (RNM) error models are analyzed and implemented for all twenty RS and the sensitivity of the monitor's performance to the RNM model is evaluated. The prototype uses the GPS legacy orbit model and does not assume a reference station clock model. Previous covariance analyses showed that the standard deviation of the monitor's orbit/clock estimation error was expected to be on the order of 30 centimeters. In this preliminarily evaluation, satellite orbits and clock errors are on the order of meters.

I INTRODUCTION

This paper describes the design, implementation and evaluation of an offline ground monitor (OFM) for aircraft navigation using future dual-frequency, multi-constellation advanced receiver autonomous integrity monitoring (ARAIM). Unlike in Satellite-Based Augmentation Systems (SBAS), fault detection (FD) using ARAIM is autonomously performed at the airborne receiver. In ARAIM, the primary goal of the OFM is to validate, over periods of several months, the assertions made at the airborne receiver.

For the global positioning system (GPS), receiver autonomous integrity monitoring (RAIM) has been used for decades to mitigate the impact of rare-event faults including satellite clock and orbit ephemeris faults in global navigation satellite systems (GNSS) [1]–[3]. The core principle of RAIM is to exploit redundant measurements to achieve self-contained FD at the user receiver [4].

With the modernization of GPS (U.S.), the full deployment of GLONASS (Russia), Galileo (European Union) and Beidou (China) [5], the number of redundant ranging signals increases dramatically, which opens the possibility to independently support worldwide aircraft navigation. This includes supporting stringent requirements for vertical guidance of aircraft down to 200 feet altitude above the runway [6]–[8]. Most importantly, by taking advantages of the revolutionary developments in GNSS, the reliance on the ground infrastructure will be alleviated in future ARAIM. This is why researchers in the European Union and in the United Sates [9], [10], are developing new dual-frequency, multi-constellation ARAIM fault detection and exclusion (FDE) methods.

To incorporate information from multiple constellations at different stages of their development, ARAIM relies on Integrity Support Messages (ISM) which is generated using OFM and broadcast to airborne receivers. The ISM provides integrity parameters describing measurement errors and faults such as for example, the prior probability of satellite faults, the prior probability of constellation-wide faults, and the standard deviation of nominal ranging measurement uncertainty due to satellite orbit and clock ephemeris errors [6], [7]. These integrity parameters are key inputs to the airborne ARAIM algorithm, which defines positioning error bounds called protection levels (PL). In current conventional RAIM implementations, these integrity parameters are defined by the GPS constellation service provider (CSP) commitments, and are hardcored in the receiver. For ARAIM implementations, the ISM parameters will be generated and validated at the ground, and updated to users as needed. Various methods of ISM dissemination are presently being considered, including broadcast on the CSP navigation message. The methods and results described in this paper are applicable regardless of the way of dissemination.

To validate the ISM, 'online' and 'offline' ARAIM architectures have been investigated [7], [11]. Offline architectures have generally been perceived as preferable because they do not require frequent communication between users and ground segment, thereby eliminates the connectivity risk [7]. An offline ARAIM monitor would rely on post-processed GNSS measurements, collected from 20 ground stations, to bound errors in the CSP broadcast navigation messages on a long-term basis. To do this, prior research utilized truth satellite positions and clock biases from the international GNSS service (IGS) network [12]–[14]. However, given that ARAIM is intended to operate over several decades, monitor dependence on external organizations with little or no stake in civil aviation must be carefully considered, and ideally, avoided. Most importantly, ARAIM will be used in safety critical applications. All potential sources of safety risk, including the monitor's truth data, must be properly accounted for. The IGS, the national geospatial intelligence agency (NGA), and others currently provide high-accuracy satellite orbit and clock products. But none of these agencies make specific commitments on the reliability of their products, or on the processes used to obtain those products. Further, data gaps exist in those products, especially during satellite fault events, which are crucial to ARAIM. In response, this paper develops a new approach to define and validate ISM parameters by designing a dedicated ARAIM offline ground monitor architecture. Estimated satellite orbit and clocks can then be differenced from the GNSS broadcast navigation message to determine satellite orbit and clock errors. This satellite orbit/clock error data will provide the means to validate the ISM parameters.

In our prior work, we designed and analyzed a dedicated ARAIM OFM [15]. The monitor employs a simple and transparent orbit determination process, intended to facilitate integrity analysis. The process is based on well-established parametric orbit models for medium-earth-orbiting satellites, which are accurate for up to four-hour time intervals. The fidelity of the orbit model was validated by quantifying residual errors relative to known satellite positions [15]. In addition, the monitor may utilize existing worldwide SBAS ground infrastructure. Twenty SBAS reference station (RS) are considered to continuously estimate satellite positions and clock biases. In [15], a covariance analysis was carried out to assess the impact of RS measurement uncertainty on satellite position and clock estimation. It indicated that the standard deviation of the monitor's estimated orbit/clock error should be on the order of 30 cm.

These results have motivated to prototype the OFM concept using experimental data, which is the focus of this work. In the following sections, the paper discusses the required OFM performance, the OFM architecture and details of the proposed estimator design.

II REQUIRED OFM PERFORMANCE

Using an OFM, the update rate of the ISM may vary from a month to multiple years depending on variations in constellation performance [7]. A large amount of data will be processed at the ground to obtain the ISM, which is expected to bound the signal-in-space (SIS) performance until the next update. To achieve this, differences between broadcast ephemeris and the monitor's estimated satellite orbit/clock will be first evaluated over time, and then these will be used to validate (or modify, if needed) the ISM parameter values. In this paper, we mainly focus on producing satellite orbit and clock estimates to validate b_{nom} and σ_{URA}, which specify a Gaussian bound on the SIS performance under nominal conditions, (i.e., no faults). Since the monitor's orbit/clock estimation errors will directly contribute to our ability validate ISM, it is necessary to first define the required accuracy of the monitor's orbit/clock estimator.

Equation (1) shows the relationship between the actual standard deviations of broadcast satellite orbit/clock error σ_{URA}, the standard deviation of the monitor's estimated orbit/clock error σ_{OFM}, and the validated standard deviation of the satellite orbit/clock error $\alpha\ \sigma_{URA}$ (validated σ_{URA}). (In the ISM, the multiplying factor α, is updated rather than σ_{URA}).

$$\alpha\sigma_{URA} = \sqrt{\sigma_{URA}^2 + \sigma_{OFM}^2} \tag{1}$$

Figure 1 shows $\alpha\ \sigma_{URA}$ vs σ_{OFM} for an example broadcast σ_{URA} value of 1 m. According to the most recent study on GPS SIS performance to support ARAIM, the maximum σ_{URA} of 1 m, or less is observed on space vehicle number (SVN) 61. And dual-constellation ARAIM availability simulations have revealed localizer performance with vertical guidance (LPV)-200 approach can only be supported when σ_{URA} of both constellations are approximately 1 m [7]. The figure shows slow growth of $\alpha\ \sigma_{URA}$ as σ_{OFM} increases. Even when σ_{OFM} reaches 0.5 m, i.e. half of σ_{URA}, the achievable validated σ_{URA} is still around 1.12 m.

In addition to σ_{OFM}, the estimated satellite orbit/clock error may have a non-zero mean, denoted by b_{OFM} . This term is accounted as one component of the validated ISM parameter, b_{nom}. However, using baseline solution separation ARAIM user

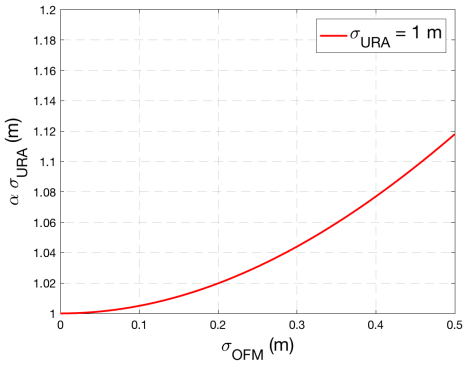

Fig. 1. Sensitivity of OFM on validating σ_{URA}

algorithm [9], the absolute value of b_{nom} is additive for each measurement. This causes the integrity risk bound to become loose as the number of measurements increases, thereby degrading availability performance [9]. Therefore, it is desirable to mitigate any contributions of b_{OFM} to the validated b_{nom}.

From the analysis and discussion above, it can be seen that the required accuracy of the offline monitor is significantly lower than the precise satellite orbit/clock products by IGS or NGA. Instead, it is the reliability of the monitor's estimator output that is key. In other words, even though the monitor's satellite orbit/clock estimates may have larger errors most of the time, their stable performance and consistent availability will enable ISM validation without data gaps, especially at crucial times when SV faults occur. Therefore, in the estimator design, it is not necessary to pursue a complicated orbit determination process. Instead a simple, transparent approach is described in the next section.

III ARCHITECTURE OF THE OFM PROTOTYPE

This section describes the OFM architecture step-by-step. A network of worldwide sparsely distributed RS is employed to collect code and carrier measurements over time. In the selection of sites for the RS, we take advantage of the SBAS ground infrastructures since they are already installed and designed to support civil aviation applications. Figure 2 shows all existing SBAS RS across the globe. For the prototype, we have selected 20 RS shown in figure 3. Because SBAS data are not publicly accessible, we use RS from the IGS network as a surrogate for SBAS RS. This network ensures that each satellite can continuously be tracked by at least 3 RS (Fewer than 3 RS could degrade the monitoring performance).

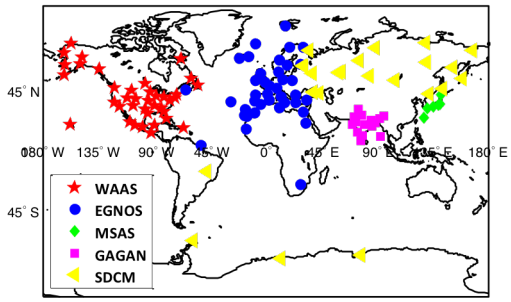

Fig. 2. ALL existing SBAS stations

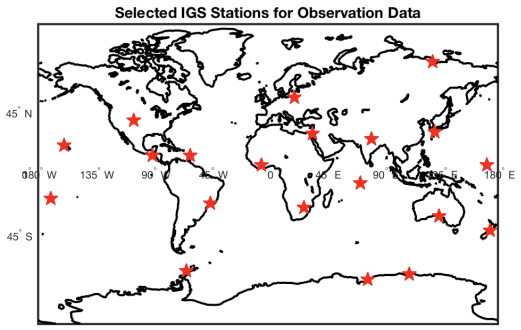

Fig. 3. Selected IGS stations for the prototype

The OFM uses parametric orbit models to determine space vehicle (SV) trajectories. In prior work, we evaluated both the 15-parameter GPS legacy orbit model and the 17-parameter CNAV model [15]. In this prototype, we assume no satellite maneuvers occurs, because the orbit models would not be valid. Maneuvers occurs rarely, and they can be handled in post-processing by simply initiating a new estimator after the maneuver. These details of monitor implementation are beyond the scope of this prototype and will not be discussed further. In this prototype, the OFM estimates GPS legacy orbit model parameters, SV clock biases and RS clock biases assuming no satellite maneuver (the GPS CNAV model will be implemented in the next steps of this work).

Let p_i^{orb} be the 15 x 1 vector of orbit parameters for SV i, and let g_k^{orb} be the non-linear function that determines SV orbit. The true SV position X_k^i of SV i at time epoch k can be expressed as:

$$X_k^i = g_k^{orb}(p_i^{orb}) + \nu_k^{orb,i} \tag{2}$$

where $\nu_k^{orb,i}$ is the deviation of model output from the true position X_k^i. $\nu_k^{orb,i}$ represents the model's inability to perfectly capture the true orbit. These model fidelity errors can be bounded by a zero-mean Gaussian distribution with a standard deviation of 12 cm when using the legacy model [15]. The GPS orbit model is valid over a four-to-six hour time interval noted T_{FIT} [16]. Sensitivity to T_{FIT} has been evaluated in our prior work in [17]. We use a four-hour fitting interval, which is the most common value for GPS ephemeris.

Both RS and SV are equipped with atomic clocks, and a quadratic polynomial can be employed to model their nominal errors. However, most SV faults are caused by their clocks, and for the monitor to clearly observe them, no assumption can be made on the SV clock dynamics. As for the RS clocks, covariance analysis indicated that the performance of OFM is not improved much with a quadratic model on RS clock errors [15]. Thus, no assumptions is made on RS clocks.

The ionospheric-free code and carrier phase measurements (dual-frequency) for SV i from RS j at time epoch k are expressed in the following two equations:

$$\rho_k^{i,j} = \|X_j - X_{i,k}\| - \tau_{i,k} + b_{j,k} + T_k^{i,j} + \varepsilon_{RNM,\rho,k}^{i,j} \tag{3}$$

$$\phi_k^{i,j} = \|X_j - X_{i,k}\| - \tau_{i,k} + b_{j,k} + \eta^{i,j} + T_k^{i,j} + \varepsilon_{RNM,\phi,k}^{i,j} \tag{4}$$

where,
X_j : known location of RS j, for example, in an Earth-Centered Earth-Fixed (ECEF) reference frame
$X_{i,k}$: unknown location of SV i at time k
$\tau_{i,k}$: unknown clock offset of SV i at time k
$b_{j,k}$: unknown clock offset of RS j at time k
$\eta^{i,j}$: unknown, constant iono-free carrier phase cycle ambiguity for SV i at RS j
$\| \ \|$: Euclidean norm operator, in this case providing the distance between RS j and SV i.
$T_k^{i,j}$: Tropospheric delay errors for SV i and RS j at time k

The error terms in equations (3) and (4) account for receiver noise and multipath (RNM) errors denoted by $\varepsilon_{RNM,\rho,k}^{i,j}$ and $\varepsilon_{RNM,\phi,k}^{i,j}$ for code and carrier respectively. The error models are described later in the Section VI.

To correct for tropospheric delay affect the data, we have considered "UNBm" Neutral Atmosphere Model (developed by University of New Brunswick, Fredericton, Canada) [18]. It shows that residuals of the "UNB3m" model are approximately a zero mean with a standard deviation of 5 cm observed throughout years. Further, these residuals are written as a function of zenith tropospheric delay (ZTD) using a mapping function (c_T) given in [7], [9], [10].

$$T_k^{i,j} = T_{i,j,k}^{model} + c_T \varepsilon_{tropo,j}^{ZTD} \tag{5}$$

To estimate the SV orbit parameters and clocks, the measurement equations (3) and (4) and the orbit model equation (2) are linearized and incorporated into a single filter. We illustrate this process for code measurements in the following derivation. Using broadcast ephemeris ($X_{i,k}^*$) and tropo model equation (5) :

$$\begin{aligned} \delta\rho_k^{i,j} &= \rho_k^{i,j} - \|X_j - X_{i,k}^*\| - T_{i,j,k}^{model} \\ &= {}^{i,j}e_k^T \delta X_{i,k} - \tau_{i,k} + b_{j,k} + c_T \varepsilon_{tropo,j}^{ZTD} + \varepsilon_{RNM,\rho,k}^{i,j} \end{aligned} \tag{6}$$

Where,
δ : deviation from nominal values, i.e $\delta X_{i,k} = X_{i,k} - X_{i,k}^*$
${}^{i,j}e_k^T$: 3 x 1 line of sight (LOS) unit vector from RS j to SV i at time k

In the next step, the orbit model is linearized at ${}^*p_i^{orb}$ where, $X_{i,k}^* = g_k^{orb}({}^*p_i^{orb})$. Substituting the linearized orbit model equation into the code measurement, equation (6) becomes:

$$\delta\rho_k^{i,j} = {}^{i,j}e_k^T \ A_{i,k}^{orb} \ \delta p_{i,k}^{orb} - \tau_{i,k} + b_{j,k} + c_T \varepsilon_{tropo,j}^{ZTD} + \varepsilon_{RNM,\rho,k}^{i,j} \tag{7}$$

Where,
$A_{i,k}^{orb}$: Jacobian matrix for the SV orbit model in equation (2), which is 3 x 15 for the GPS legacy orbit model. It is composed of numerically-derived partial derivatives of the position coordinates of SV i at time k, $X_{i,k} = [x_{i,k} \quad y_{i,k} \quad z_{i,k}]^T$ with respect to the orbit parameters $p_i^{orb} = [p_1 \quad \cdots \quad p_{15}]^T$

$$A_{i,k}^{orb} = \begin{bmatrix} \frac{\partial x_{i,k}}{\partial p_1} & \cdots & \frac{\partial x_{i,k}}{\partial p_{15}} \\ \frac{\partial y_{i,k}}{\partial p_1} & \cdots & \frac{\partial y_{i,k}}{\partial p_{15}} \\ \frac{\partial z_{i,k}}{\partial p_1} & \cdots & \frac{\partial z_{i,k}}{\partial p_{15}} \end{bmatrix}_{3x15} \tag{8}$$

In addition, the product of line-of-sight vector and Jacobian matrix is defined as,

$$B_k^{i,j} \triangleq {}^{i,j}e_k^T A_{i,k}^{orb} \tag{9}$$

Equation (7) becomes:

$$\delta\rho_k^{i,j} = B_k^{i,j}\delta p_{i,k}^{orb} - \tau_{i,k} + b_{j,k} + c_T\varepsilon_{tropo,j}^{ZTD} + \varepsilon_{RNM,\rho,k}^{i,j} \tag{10}$$

Similarly, the linearized carrier phase measurement can be written as,

$$\delta\phi_k^{i,j} = B_k^{i,j}\delta p_{i,k}^{orb} - \tau_{i,k} + b_{j,k} + \eta^{i,j} + c_T\varepsilon_{tropo,j}^{ZTD} + \varepsilon_{RNM,\phi,k}^{i,j} \tag{11}$$

IV ESTIMATOR DESIGN

We design the estimator for the linearized measurements in equations (10) and (11). The parameters to be estimated or 'states' include SV orbit parameters δp_i^{orb}, SV clock $\tau_{i,k}$, RS clock $b_{j,k}$, cycle ambiguities $\eta^{i,j}$ and zenith tropospheric delay residual $\varepsilon_{tropo,j}^{ZTD}$. An information smoother is implemented to simultaneously estimate these states over T_{FIT} of 4 hours. A sample period of 4 minutes is selected assuming that, at such infrequent intervals, measurement error correlation due to RS multipath would be negligible.

Measurement model

$$\begin{bmatrix} \delta\rho^{1,1} \\ \delta\rho^{1,2} \\ \vdots \\ \delta\rho^{1,20} \\ \delta\rho^{2,1} \\ \vdots \\ \delta\rho^{32,20} \\ \delta\phi^{1,1} \\ \vdots \\ \delta\phi^{32,20} \end{bmatrix}_k = \begin{bmatrix} B^{1,1} & \cdots & 0 \\ B^{1,2} & \cdots & 0 \\ \vdots & & \vdots \\ B^{1,20} & \cdots & 0 \\ 0 & B^{2,1} \cdots & 0 \\ & \ddots & \\ 0 & \cdots & B^{32,20} \\ B^{1,1} & \cdots & 0 \\ & \ddots & \\ 0 & \cdots & B^{32,20} \end{bmatrix} \begin{bmatrix} 1 & \cdots & 0 \\ 1 & \cdots & 0 \\ \vdots & \cdots & \vdots \\ 1 & \cdots & 0 \\ 0 & 1 \cdots & 0 \\ & \ddots & \\ 0 & & 1 \\ 1 & \cdots & 0 \\ & \ddots & \\ 0 & \cdots & 1 \end{bmatrix} \begin{bmatrix} 0 & \cdots & 0 \\ 1 & \cdots & 0 \\ & \ddots & \\ 0 & \cdots & 1 \\ 0 & \cdots & 1 \\ & \ddots & \\ 0 & \cdots & 1 \\ 0 & \cdots & 1 \\ & \ddots & \\ 0 & \cdots & 1 \end{bmatrix} \begin{bmatrix} 0 & \cdots & 0 \\ 0 & \cdots & 0 \\ \vdots & & \vdots \\ 0 & \cdots & 0 \\ 0 & \cdots & 0 \\ & \ddots & \\ 0 & \cdots & 0 \\ 0 & \cdots & 0 \\ & \ddots & \\ 0 & \cdots & 0 \end{bmatrix} \begin{bmatrix} c_T & \cdots & 0 \\ 0 & c_T & \cdots & 0 \\ \vdots & & \ddots & \vdots \\ 0 & & & c_T \\ 0 & c_T & \cdots & 0 \\ & & \ddots & \\ 0 & & & c_T \\ c_T & \cdots & 0 \\ & \ddots & \\ 0 & & c_T \end{bmatrix}_k \begin{bmatrix} \delta p_1^{orb} \\ \vdots \\ \delta p_{32}^{orb} \\ \tau_1 \\ \vdots \\ \tau_{32} \\ b_2^{clk} \\ \vdots \\ b_{20}^{clk} \\ \eta^{1,1} \\ \vdots \\ \eta^{32,20} \\ \varepsilon_{tropo,1}^{ZTD} \\ \vdots \\ \varepsilon_{tropo,20}^{ZTD} \end{bmatrix}_k + \begin{bmatrix} \varepsilon_\rho^{1,1} \\ \varepsilon_\rho^{1,2} \\ \vdots \\ \varepsilon_\rho^{1,20} \\ \varepsilon_\rho^{2,1} \\ \vdots \\ \varepsilon_\rho^{32,20} \\ \varepsilon_\phi^{1,1} \\ \vdots \\ \varepsilon_\phi^{32,20} \end{bmatrix} \tag{12}$$

For time epoch k, code and carrier measurements are collected from RS 1 to 20 for all PRN (SV) 1 to 32 and stacked in a linearized measurement vector in equation (12). Estimator states are grouped and identified using different colors: green for orbit parameter, yellow for SV clock bias, gray for RS clock bias, blue for ambiguities and orange for zenith tropospheric delay (ZTD) residual. The first and second superscript represent SV and RS respectively. Since measurements are written for time epoch k, all terms are scalar except the orbit parameter terms (δP_i^{orb}): 15×1 and $B^{i,j}$: 1×15. There is one important aspect to point out; the determination of the satellite and receiver clock bias can only be made in a differential way so a time

reference must be implicitly established. In the framework of this prototype, RS 1 is considered as the reference. Thus, b_1^{clk} is not included in the state vector of equation (12).

It is important to note that not all SV will be visible to all RS for time epoch k. To lighten the notations, these cases are not explicitly expressed in equation (12). But the corresponding rows must be removed whenever the measurements are unavailable. And, the equation (12) is simplified by respectively defining Z, H, N and ε as the measurement vector, observation matrix, state vector, and error vector.

$$Z_k = H_k N_k + \varepsilon_k \tag{13}$$

Dynamic model

$$\begin{bmatrix} \delta p^{orb} \\ \tau \\ b^{clk} \\ \eta \\ \varepsilon_{tropo}^{ZTD} \end{bmatrix}_{k+1} = \begin{bmatrix} \mathbb{I} & 0 & 0 & 0 & 0 \\ 0 & \mathbb{I} & 0 & 0 & 0 \\ 0 & 0 & \mathbb{I} & 0 & 0 \\ 0 & 0 & 0 & \mathbb{I} & 0 \\ 0 & 0 & 0 & 0 & e^{-T/\mu}\,\mathbb{I} \end{bmatrix} \begin{bmatrix} \delta p^{orb} \\ \tau \\ b^{clk} \\ \eta \\ \varepsilon_{tropo}^{ZTD} \end{bmatrix}_k + \begin{bmatrix} 0 & 0 & 0 \\ \mathbb{I} & 0 & 0 \\ 0 & \mathbb{I} & 0 \\ 0 & 0 & 0 \\ 0 & 0 & \mathbb{I} \end{bmatrix} \begin{bmatrix} \omega_\tau^{clk} \\ \omega_b^{clk} \\ \omega_{tropo}^{ZTD} \end{bmatrix} \tag{14}$$

$$N_{k+1} = \phi N_k + \Gamma \omega_k \tag{15}$$

The color-code for the terms highlighted in equation (14) is consistent with equation (12). But equation (14) is written in vector-form by stacking together the corresponding scalar quantities. The orbit parameters are constant throughout T_{FIT}. Since our goal is to estimate clocks instantaneously, infinite process noise is added so that both SV and RS clock knowledge does not be propagated to the next time epoch. Thus, the estimator completely relies on the measurements for determining the clock states. Cycle ambiguities are constant but will be reset if cycle slip occurs. The ZTD residuals, in the last row, are treated as First Order Gauss Markov Processes where T is the sample period, μ is the time constant [19] and the variance of ω_{tropo}^{ZTD} is $(1 - e^{-2T/\mu})\sigma_{ZTD}^2$.

Nominal Information Filter steps can be implemented to estimate SV orbit parameters. During the first few time-steps when running the filter, the estimated SV and RS clock biases are not poor. To get better estimates of the clock bias states, especially in these first few time steps, a backward information filter is run. The forward and backward filter together are referred to as the information smoother. The main advantages of this implementation are its time and memory-efficiency and the fact that no prior knowledge on any states except on the ZTD residual error.

The SV i's orbit parameters δP_i^{orb} and clock bias $\tau_{i,k}$ can be extracted from the estimated state vector $\hat{N}_k$. Furthermore, the SV position is obtained by substituting the estimated orbit parameter into equation (2).

V COVARIANCE ANALYSIS

In this section, a covariance analysis illustrates the contribution of measurement error on σ_{OFM}. The information smoother provides an estimated state covariance matrix $\hat{\Sigma}_k$. To validate the ISM, we only need SV orbit parameters and clock information; the corresponding elements can be extracted from $\hat{P}_k$. For example, SV i's orbit parameters and clock bias at time epoch k are extracted and arranged in a vector labeled $D_{i,k}$ with dimension of 16×16. Then, the 4×4 covariance matrix $\hat{P}_{LL,i,k}$ of the satellite position and clock in the local-level (LL) reference frame (along-track, cross-track, radial) can be evaluated using the following equation:

$$\hat{P}_{LL,i,k} = \begin{bmatrix} R_{LL,i,k} & 0 \\ 0 & 1 \end{bmatrix} C_{i,k} D_{i,k} C_{i,k}^T \begin{bmatrix} R_{LL,i,k} & 0 \\ 0 & 1 \end{bmatrix}^T \tag{16}$$

where $R_{LL,i,k}$ is the ECEF to LL rotation matrix, and $C_{i,k}$ is defined as:

$$C_{i,k} = \begin{bmatrix} A_{i,k}^{orb} & 0 \\ 0 & 1 \end{bmatrix} \tag{17}$$

To investigate the SIS performance in the range domain, we evaluate the maximum Signal-In-Space Ranging Error (SISRE) standard deviation at the worst-case user location. This is achieved by projecting $\hat{P}_{LL,i,k}$ along line-of-sights for all locations within SV footprint [12]. And the worst-case SISRE standard deviation $\sigma^{SISRE,i,k}$ is defined as the maximum standard deviation over all of these locations. In Figure 4, the projection region is shaded in light blue, and the black dashed line is one example projection line $G_{i,m}$, where m is the index of the user location. Therefore, $\sigma^2_{SISRE,i,k}$ is given by:

$$\sigma^2_{SISRE,i,k} = \max_{m=i,\ldots,ALL} (G_{i,m} \hat{P}_{LL,i,k} G^T_{i,m}) \tag{18}$$

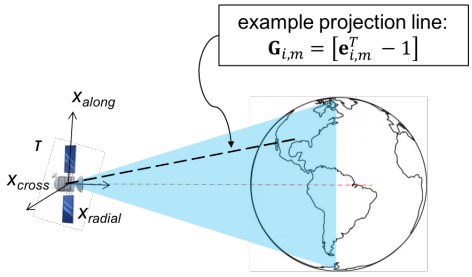

Fig. 4. Covariance matrix projection along LOS for all locations

VI ERROR MODEL

For the OFM prototype, we collected code and carrier measurements from 20 IGS stations (Figure 3). Since code RNM error is the largest source of error in OFM data, we start by characterizing code measurements using ionospheric-free code-minus-carrier (CMC) observations. We develop individual code error models for each 20 IGS stations. RNM errors are evaluated as a function of elevation. For example, Table I shows RNM code errors for one of the IGS station (station code - 'kokv'). Below 10 degree elevation, few measurements are available. Therefore, the prototype uses measurements above 10 degree elevation. More detailed explanation on RNM error modeling are given in Appendix A. Overall for all IGS RS, iono-free code RNM errors are overbounded by Gaussian distribution with zero mean and standard deviations of 1 m to 3 m depending on elevation angle.

TABLE I
CODE ERROR MODEL FOR IGS RS 'KOKV'

Elevation (deg.)		Mean (m)	Bounded sigma (m)	No of samples
Min.	Max.			
0	10	0.29	4.11	35
10	15	0.07	2.79	1067
15	20	0.02	2.55	2250
20	25	0.07	1.88	3069
25	30	0.06	1.49	2338
30	35	0.01	1.22	2127
35	40	0.08	1.05	2231
40	90	0.06	1.06	10669

In the next section VII, we will show that the performance of the OFM is less sensitive to carrier phase RNM error than it is to code RNM error. Therefore, we assume a simple, conservative model for carrir RNM: we assume that raw L1 carrier phase noise can be overbounded by a Gaussian distribution with zero mean and standard deviation of 1 cm. Taking into account the noise inflation due to iono-free carrier noises (L1/L2), the standard deviation of carrier measurements in equation (12) becomes 2.98 cm. In the next steps of this work, we will perform a more accurate analysis of carrier errors.

In addition, we assumed that the tropo model (UNB3m [18]) was valid for all IGS RS and that the ZTD residual errors could be modeled using a First-order Gauss Markov Process with zero mean, a standard deviation of 5 cm and a time constant of 2 hours. In future steps, we will analyze ZTD residual errors for all RS. If the current model is not sufficient, we may utilize local weather information (temperature, pressure, relative humidity) to estimate precise tropospheric delay corrections.

VII SENSITIVITY ANALYSIS

To achieve SV orbit and clock determination with sub-meter precision, we need to consider sensitive parameters and we must quantify their impact on the OFM.

VII-A Impact of code error model

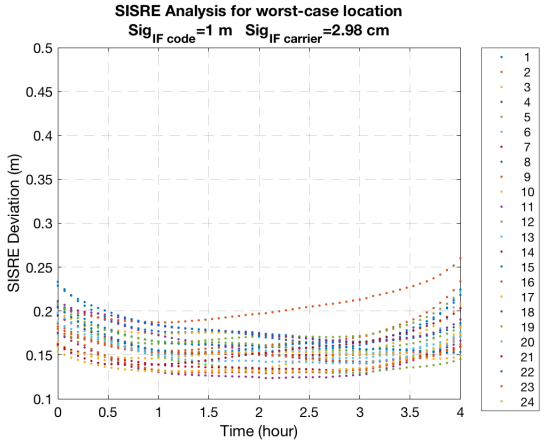

Fig. 5. Covariance analysis using precise code error model

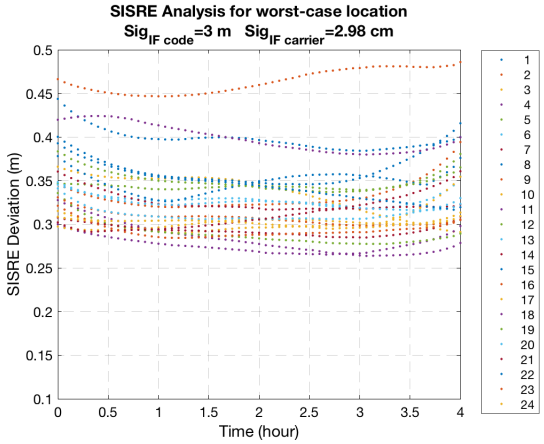

Fig. 6. Covariance analysis using noisy code error model

The sensitivity of the OFM to error model parameters is illustrated using a straightforward covariance analysis, by changing code RNM error model parameter values while keeping all other parameters constant. SISRE deviations are shown for 24 SV in different colors in Figures 5 and 6. In Figure 5, we model code RNM errors as zero-mean normally-distributed with 1 m standard deviation for all SV elevations. In contrast, in Figure 6, a 3 m standard deviation is assumed for all SV elevations. The two figures show that the OFM is sensitive to code RNM error. Thus, we put significant amount of effort to develop precise code error model for each 20 IGS stations for the prototype.

VII-B Impact of carrier error model

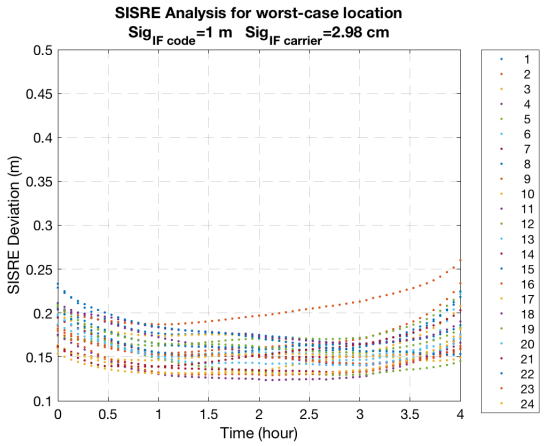

Fig. 7. Covariance analysis using precise carrier error model

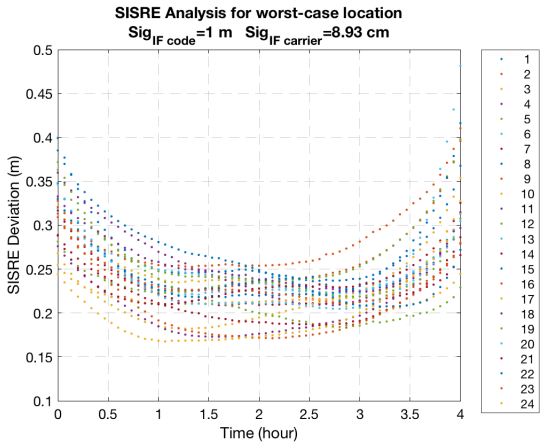

Fig. 8. Covariance analysis using noisy carrier error model

Similarly, the sensitivity of carrier phase RNM errors is analyzed by changing the error model standard deviation on iono-free carrier from 2.98 cm (in Figure 7) to 5.18 cm (8). (In both cases, we assume a constant 1 m standard deviation on code RNM errors at all SV elevations.) The two figures show that the OFM monitor performance is less sensitive to carrier errors than it is to code errors. Therefore, the current prototype uses an iono-free carrier error model with a 2.98 cm standard deviation.

VII-C Synchronizing RS clocks

At a given true GPS time t, the iono-free code measured for RS j can be expressed as:

$$\rho^{i,j} = \|X_j - X_i\| - \tau_i + b_j + T^{i,j} + \varepsilon^{i,j}_{RNM,\rho} \tag{19}$$

This measurement is timetagged at RS receiver time, $t^j(t)$, which is related to GPS time as expressed in the following equation:

$$t^j(t) \triangleq \frac{b_j(t)}{c} + t \tag{20}$$

Similarly, at the RS m, iono-free code measurements are timetagged using RS m's receiver time, $t^m(t)$, which is related to GPS time as expressed in the following equation:

$$t^m(t) \triangleq \frac{b_m(t)}{c} + t \tag{21}$$

where, $b_m(t)$ is the RS m's receiver clock bias expressed in unit length (in meters). Measurements with identical timetags are actually collected at different times.

Some receivers uses code phase measurements to perform internal position and clock bias estimation. The receiver is designed to use the resulting estimated receiver clock bias to adjust the receiver clock within ±0.5 msec of GPS time. Therefore, the maximum time-difference between the RS j and RS m times is limited to 1 msec. However, considering that the satellite-to-receiver range rate (doppler) can exceed 1000 m/s, deviations of greater than 1 m are still possible in both code and carrier measurements. Therefore, a time-alignment procedure is necessary because the prototype aims at achieving sub-meter precision. This point is further described in Appendix B. For prototype implementation, a modification is applied to the receiver clock bias states (gray highlighted area in equation (12)) as shown below.

$$\delta\rho^{i,j}_k = B^{i,j}_k \delta p^{orb}_{i,k} - \tau_{i,k} + \frac{c - \dot{\phi}_k}{c} b_{j,k} + c_T \varepsilon^{ZTD}_{tropo,j} + \varepsilon^{i,j}_{RNM,\rho,k} \tag{22}$$

where, c is speed of light and $\dot{\phi}$ is doppler rate.

VII-D Modifying the GPS Legacy orbit model for the OFM

This subsection addresses a numerical issue caused by two singularities in the GPS legacy orbit model that we use in the OFM estimator. The first singularity occurs when the satellite orbit is circular (eccentricity (e) equal to zero). In this case, the line of apsis and the argument of perigee ω are undefined. The second singularity occurs when the orbit is equatorial (inclination equal to zero). In this case, the ascending node and the right ascension of ascending node Ω are unidentified.

In order to prevent convergence problems when the eccentricity is close to zero, the following change of variable was considered [20].

$$\begin{aligned} L &= \omega + M_0 \\ e_Y &= e * sin\omega \\ e_X &= e * cos\omega \end{aligned} \tag{23}$$

where, M_0 is mean anomaly.

Instead of estimating ω, e, M_0, the prototype will estimate parameters L, e_X, e_Y. Additional detail about our implementation is provided in Appendix C.

VIII RESULTS

We use raw code and carrier measurements from 20 IGS station to evaluate our prototype OFM. The reported RS locations are obtained from the header of the Receiver Independent Exchange Format (RINEX) input file. (The RINEX is a data interchange format for raw satellite navigation system data.) These location estimates are approximate and will need to be validated in the future work. To run the proposed information smoother, data is taken over 4 hours periods with a sample interval of 4 minutes. The information smoother is executed using equations (12) and (14). As a result, for a given SV and over a 4-hour

period, we will obtain 15 orbit parameters and a SV clock bias every 4 minutes. (RS clock biases and cycle ambiguities are also obtained but are not needed for validating the ISM). To validate the estimated parameters, we use the NGA 'orbit product' which provides SV orbit and clock biases with an accuracy of 2.5 cm. One important point is that the NGA orbit position is given at the SV antenna phase center (APC) while IGS products are referenced to the center of mass (C.M.). The legacy orbit model captures the position of the APC. Therefore, our estimated orbit parameters are referenced to the APC and will be compared with the NGA orbit product.

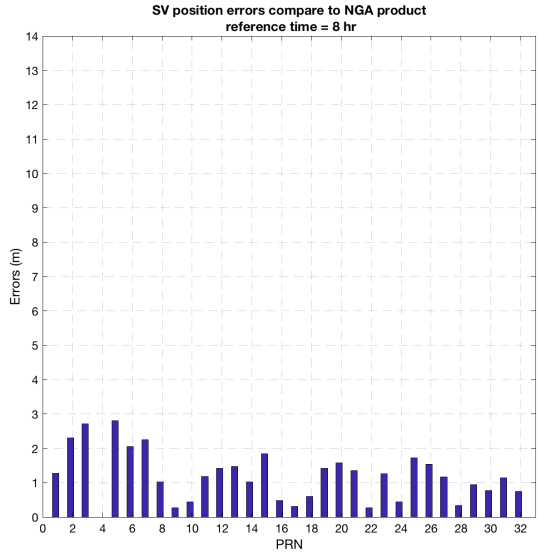

Fig. 9. Comparing estimated SV position with NGA product

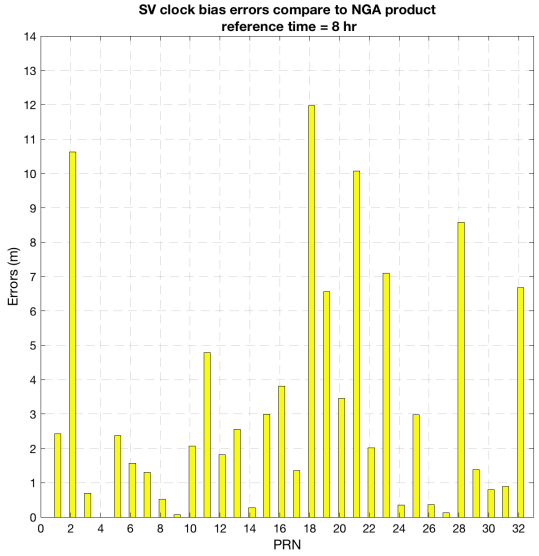

Fig. 10. Comparing estimated SV clock bias with NGA product

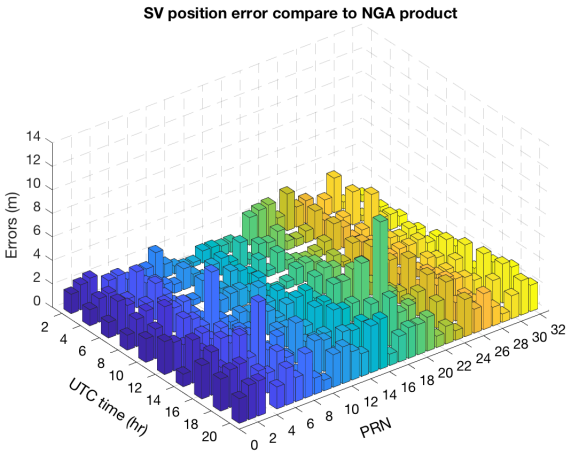

Fig. 11. Estimated SV position error over a day

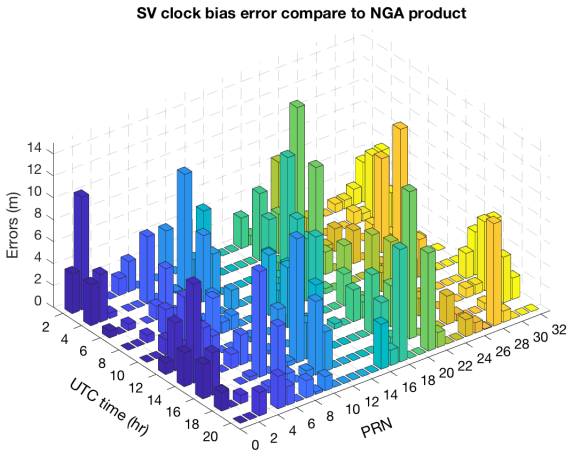

Fig. 12. Estimated SV clock bias error over a day

To evaluate the OFM performance, measurements from UTC 6:00 to 10:00 on 1-3-2018 are fed into the information smoother. Estimated orbit parameters will be most accurate during the central two hours of the fitting period (between 7:00 and 9:00). To make the comparison simpler, SV orbit and clock biases are extracted for UTC 8:00 and compared to the NGA product. Figure 9 shows the error magnitude of SV orbit in the x,y,z direction for all 32 visible 32 PRNs. These errors are larger than our desired 0.3 m error but these are preliminary results. It is still remarkable to achieve meter-level of orbit error without considering any prior information in the orbit model. It is worth noting that the estimated clocks are reference to RS 1 while the NGS clock bias is referenced to GPS time. To make a comparison, the mean of the constellation clock bias is removed for

a specific time epoch k. For example, the mean of the estimated SV clock biases for 32 PRNs is computed for UTC 8:00 and referred to as the constellation's mean. Similarly, the mean of SV clock biases from the NGA product is also computed for UTC 8:00. The corresponding constellation mean for the OFM and for the NGA is removed from individual SV clock biases and differenced to evaluate errors displayed in Figure 10. These are large errors, which we hope can be reduced in the future work.

In Figures 9 and 10, we evaluated the OFM performance for a single 4-hour fit interval. In Figure 11 and 12, we slide the time window (T_{FIT}) over an entire day on 1-3-2016. Figure 11 shows the magnitude of orbit errors on estimator over that day. In parallel, Figure 12 shows the SV clock estimation errors. Note that, for each time epoch, the constellation mean clock is removed as described above. The maximum SV orbit error and clock bias are observed close to 10 m and 14 m over a day respectively.

This preliminary result shows errors larger than our desired 0.3 m. However, multiple adjustments can be performed to improve the prototype orbit and clock determination process, including using more accurate carrier error model, RS location estimates, and tropospheric delay models.

IX CONCLUSION

This paper describes the design, sensitivity analysis, and preliminary evaluation of an ARAIM offline ground monitor prototype, which aims at validating the ISM broadcast to ARAIM users. The monitor employs a worldwide network of sparsely-distributed reference stations (RS) and a parametric orbit model to simultaneously estimate SV obits, SV clock biases, and RS clock biases. An information smoother is implemented for time and memory efficiency. Moreover, the GPS legacy orbit model is modified for numerical stability of the estimator. In the sensitivity analysis, the impact of the error model is discussed and code-phase error models are developed for all 20 IGS stations whose data are used in this prototype. Preliminarily results show that the estimated SV orbit and clock errors over one day do not exceed 10 meters and 14 meters, respectively. In the next steps, we will validate the RS locations, implement more accurate models for residual tropospheric errors and carrier-phase errors and we will model the time-correlation of code and carrier errors to run the estimator at higher sampling rates. Further, the CNAV model will be implemented to improve orbit determination performance.

ACKNOWLEDGMENT

The authors would like to thank the Federal Aviation Administration (FAA) for their continued support of this research effort. The opinions in this paper are our own and do not represent those of the FAA, any other person or organization.

Appendix A
CHARACTERIZATION OF CODE RNM ERROR

Raw L1 and L2 code phase measurements were collected from website: ftp://cddis.gsfc.nasa.gov/gnss/data/daily . The characterization of code measurement error can be carried out by computing code minus carrier (CMC). Since prototype utilizes iono-free code measurement, we directly compute iono-free CMC to observe residual. We have analyzed 20 IGS stations and developed code error model for each RS. To illustrate the nominal case, we will show the characterization for Hawaii station (station code is 'kokv') only. Similar procedure has been applied for other RS.

The code phase residual for satellite i is computed using following equation,

$$\text{Residual} = \rho_{IF} - \phi_{IF} + \eta_{IF} = \varepsilon_{\rho_{IF},RNM} \tag{24}$$

Figure 13 shows the residual computed for 24 hour period of January 3rd, 2016. Since larger errors are observed than expected, we put inclusion criteria for selecting measurement such as carrier noise ratio (C/N0) must be above 34 dB-Hz for L1 and 23 dB-Hz for L2. Figure 14 shows the residuals after applying inclusion criteria. Further, it is observed that the residuals are highly correlated with elevation angle as shown in figure 15. Thus, the residuals are categories in the elevation range as shown in table I. And, we use the folded cumulative distribution function (folded-CDF) bounding method to evaluate the error model for each elevation range [21]. In folded CDF representation, the empirical CDF is computed for the data and then compared to a Gaussian CDF with specific mean and standard deviation. Folded in this context means that the left tail

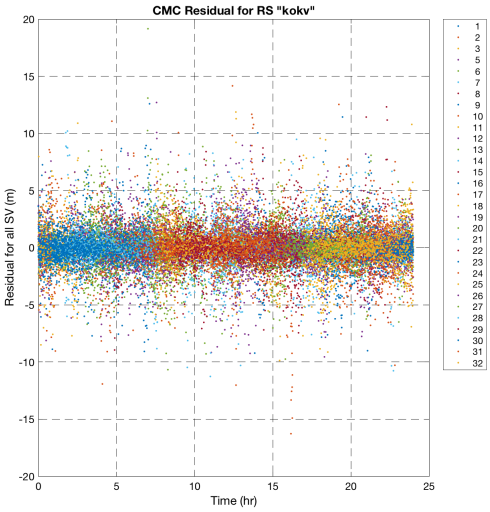

Fig. 13. Code residual without inclusion criteria

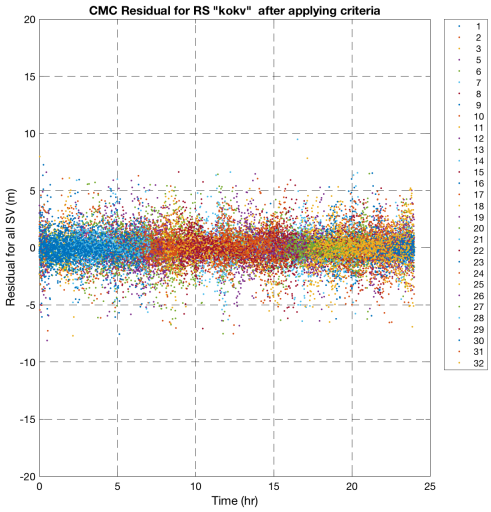

Fig. 14. Code residual with inclusion criteria

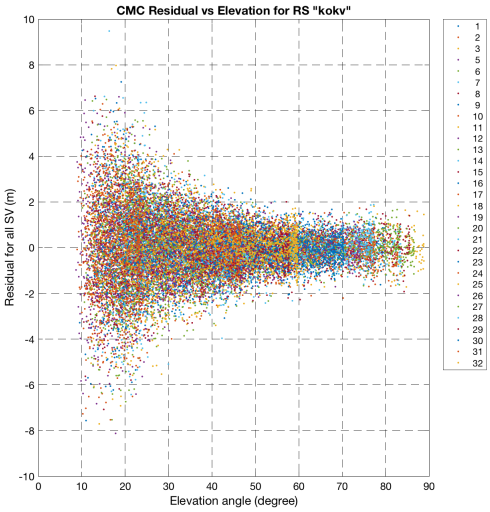

Fig. 15. Code residual as a function of elevation angle

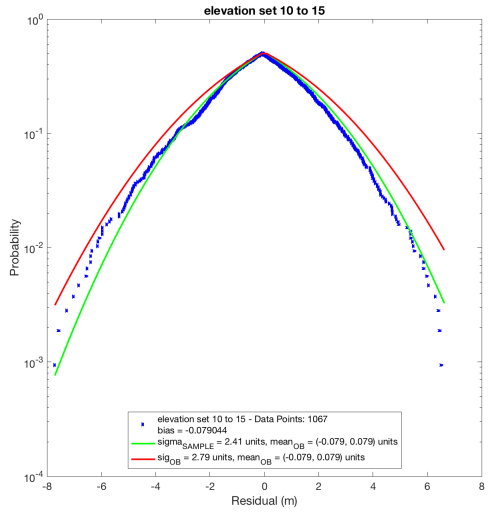

Fig. 16. Folded CDF bound for code residual of elevation set 10 to 15

likelihood is computed for errors less than median and the right tail likelihood is computed for the ones larger than the median. The Gaussian CDF with the mean and standard deviation values that overbound all empirical CDF points is referred to as the bounding Gaussian distribution, and will be used for error modeling. For example, figure 16 shows the folded CDF for residuals having elevation angle 10 to 15 degree for all visible Satellite. Similarly error model is generated for each elevation range and table I is obtained.

Appendix B
SYNCHRONIZING THE REFERENCE STATION (RS) CLOCKS

At a given true GPS time t, the iono-free carrier measured for RS j can be expressed, in meter, following equation (19), as

$$\phi^{i,j} = \|X_j - X_i\| - \tau_i + b_j + \eta_{IF} + T^{i,j} + \varepsilon^{i,j}_{RNM,\phi} \tag{25}$$

This measurement is timetagged at RS receiver time, $t^j(t)$, which is related to GPS time as expressed in the following equation:

$$t^j(t) \triangleq \frac{b_j(t)}{c} + t \tag{26}$$

Similarly, at the RS m, iono-free carrier measurements are timetagged using RS m's receiver time, $t^m(t)$, which is related to GPS time as expressed in the following equation:

$$t^m(t) \triangleq \frac{b_m(t)}{c} + t \tag{27}$$

where, $b_m(t)$ is the RS m's receiver clock bias expressed in unit length (in meters). Measurements with identical timetags are actually collected at different times.

Considering the RS j as master station and all other RS are aligned to time $t^j(t)$. For instance, RS m and RS j with same timetag,

$$t^j(t) = t^m(t_0) \tag{28}$$

where, t_0 is the true time when measurement is observed.

Now, measurement for RS m for time t_0

$$\phi^{i,m}(t_0) = \|X_m - X_i(t_0)\| - \tau_i(t_0) + b_j(t_0) + \eta_{IF} + T^{i,j} + \varepsilon^{i,j}_{RNM,\phi} \tag{29}$$

Performing a Taylor Series expansion of $\phi^{i,m}$ about t_0,

$$\phi^{i,m}(t) = \phi^{i,m}(t_0) + \frac{d}{dt}\phi^{i,m}(t_0)\,(t - t_0) + \frac{1}{2}\frac{d}{dt^2}\phi^{i,m}(t_0)\,(t - t_0)^2 + \ldots \tag{30}$$

Because the second and higher order terms contribute less than 0.1 mm, they can be neglected. Using equation (27) to express the derivative in RS m receiver time, equation (30) can be rewritten as

$$\phi^{i,m}(t) = \phi^{i,m}(t_0) + \Big[1 + \frac{1}{c}\frac{d}{dt}b_m(t_0)\Big]\frac{d}{dt^m}\phi^{i,m}(t_0)\,(t - t_0) \tag{31}$$

The term $\frac{1}{c}db_m(t_0)/dt$ is typically on the order of 10^{-6} or less. Its contribution is extremely small (< 0.01 mm) and can be neglected. Using equation (26,27,28)

$$t - t_0 = \frac{1}{c}\Big(- [b_j(t) - b_m(t)] - [b_m(t) - b_m(t_0)]\Big) \tag{32}$$

Ignoring the second term when (32) is substituted into (31) will result in an error smaller than 0.01 mm. Making this substitution and rearranging the result, the following is obtained:

$$\phi^{i,m}(t_0) = \phi^{i,m}(t) - \frac{1}{c}\frac{d}{dt^m}\phi^{i,m}(t_0)[b_m(t) - b_j(t)] \tag{33}$$

The second term represents the correction term for timetag alignment. In the prototype, RS 1 is considered as reference clock and applied implicitly. Similarly, equation (33) can be written as below and correction is applied on the prototype.

$$\phi^{i,m}(t_0) = \|X_m - X_i(t)\| - \tau_i + \left(1 - \frac{1}{c}\frac{d}{dt^m}\phi^{i,m}(t_0)\right)b_m(t) + \eta_{IF} + T^{i,j} + \varepsilon^{i,j}_{RNM,\phi} \tag{34}$$

Appendix C
MODIFIED LEGACY MODEL

The modified orbit parameters are,

$$\begin{aligned} L &= \omega + M_0 \\ e_Y &= e * sin\omega \\ e_X &= e * cos\omega \end{aligned} \tag{35}$$

With this system, chain rule is applied to get following equation:

$$\begin{bmatrix} \frac{\partial f}{\partial e_X} \\ \frac{\partial f}{\partial e_Y} \\ \frac{\partial f}{\partial L} \end{bmatrix} = \begin{bmatrix} \cos\omega & -\frac{\sin\omega}{e} & \frac{\sin\omega}{e} \\ \sin\omega & \frac{\cos\omega}{e} & -\frac{\cos\omega}{e} \\ 0 & 0 & 1 \end{bmatrix} \begin{bmatrix} \frac{\partial f}{\partial e} \\ \frac{\partial f}{\partial \omega} \\ \frac{\partial f}{\partial M0} \end{bmatrix} \tag{36}$$

Now, actual orbit parameters are replaced in Jacobian matrix, equation (8), using equation (36) for modified parameters. As a result, estimator will predict deviation in modified orbit parameters. Finally, actual legacy model parameters are obtained using following equation,

$$\begin{aligned} \hat{e} &= \sqrt{\hat{e}_X^2 + \hat{e}_{Y,new}^2} \\ \hat{\omega} &= atan2(\hat{e}_Y, \hat{e}_X) \\ \hat{M0} &= \hat{L} - \hat{\omega} \end{aligned} \tag{37}$$

References

[1] Lee, Y. C., "Analysis of Range and Position Comparison Methods as a Means to Provide GPS Integrity in the User Receiver," Proceedings of the 42nd Annual Meeting of The Institute of Navigation, Seattle, WA, 1986, pp. 1-4.

[2] Parkinson, B. W., and Axelrad, P., "Autonomous GPS Integrity Monitoring Using the Pseudorange Residual," NAVIGATION: Journal of the Institute of Navigation, Vol. 35, No. 2, 1988, pp. 255–274. doi:10.1002/j.2161-4296.1988.tb00955.x

[3] RTCA Special Committee 159, "Minimum Operational Performance Standards for Airborne Supplemental Navigation Equipment Using Global Positioning System (GPS)," RTCA/DO-208, July 1991.

[4] Joerger, M., Chan, F.-C., and Pervan, B., "Solution Separation Versus Residual-Based RAIM," NAVIGATION: Journal of the Institute of Navigation, Vol. 61, No. 4, Winter 2014, pp. 273-291. doi: 10.1002/navi.71

[5] Gibbons, G., "Munich Summit Charts Progress of GPS, GLONASS, Galileo, Beidou GNSSes," Inside GNSS, March 20, 2012.

[6] EU-US Cooperation on Satellite Navigation, WG CARAIM Technical Subgroup, "ARAIM Technical Subgroup Interim Report, Issue 1.0", 2012. URL: http://www.gps.gov/policy/cooperation/europe/2013

[7] EU-U.S. Cooperation on Satellite Navigation, Working Group C, "ARAIM Technical Subgroup Milestone 2 Report," February 11, 2015. URL: http://www.gps.gov/policy/cooperation/europe/2015/working-group-c/

[8] Blanch, J., T. Walter, P. Enge, S. Wallner, F. A. Fernandez, R. Dellago, R. Ioannides, I. F. Hernandez, B. Belabbas, A. Spletter, M. Rippl, "Critical Elements for a Multi-Constellation Advanced RAIM," NAVIGATION, Vol. 60, No. 1, 2013, pp. 53-69.

[9] Blanch, J., Walter, T., Enge, Per., Lee, Y., Pervan, B., Rippl, M., Spletter, A., and Kropp, V., "Baseline Advanced RAIM User Algorithm and Possible Improvements," IEEE Transactions on Aerospace and Electronic Systems, Vol 51, January 2015, pp. 713- 732. doi: 10.1109/TAES.2014.130739

[10] Phase II of the GNSS Evolutionary Architecture Study, February 2010. URL: https://www.faa.gov/about/office_org/headquarters_offices/ato/service_units/techops/navservices/gnss/library /documents/media/G EASPhaseII_Final.pdf

[11] Blanch, J., et al, "Architectures for Advanced RAIM: Offline and Online," Proceedings of the 27th International Technical Meeting of The Satellite Division of the Institute of Navigation (ION GNSS+ 2014), Tampa, Florida, September 2014, pp. 787-804.

[12] Walter, T., Blanch, J., "Keynote: Characterization of GNSS Clock and Ephemeris Errors to Support ARAIM," Proceedings of the ION 2015 Pacific PNT Meeting, Honolulu, Hawaii, April 2015, pp. 920-931.

[13] Perea, S., Meurer, M., Rippl, M., Belabbas, B., and Joerger, M., "URA/SISA Analysis for GPS and Galileo to Support ARAIM," NAVIGATION: Journal of the Institute of Navigation, Vol. 64, No. 2, Summer 2017, pp. 237-254. doi: 10.1002/navi.199.

[14] Walter, T., Gunning, K., Blanch, J., "Keynote: Validation of the Unfaulted Error Bounds for ARAIM," Proceedings of the ION 2017 Pacific PNT Meeting, Honolulu, Hawaii, May 2017, pp. 1-19.

[15] Zhai, Y., Joerger, M., Pervan, B., "A Dedicated ARAIM Ground Monitor to Validate the Integrity Support Message," Proceedings of Institute of Navigation GNSS+ 2017 Conference, Portland, OR, Sep 2017, pp, 1063-1076.

[16] Global Positioning System Directorate Systems Engineering and Integration, "Interface Specification IS-GPS-200," Revision H, 2013. URL: http://www.gps.gov/technical/icwg/IS-GPS-200H.pdf

[17] Joerger, M., Zhai, Y., Pervan, B., "Online Monitor Against Clock and Orbit Ephemeris Faults in ARAIM," Proceedings of the ION 2015 Pacific PNT Meeting, Honolulu, Hawaii, April 2015, pp. 932-945.

[18] Leandro R.F., M.C. Santos, and R.B. Langley (2006). UNB Neutral Atmosphere Models: Development and Performance. Proceedings of ION NTM 2006, the 2006 National Technical Meeting of The Institute of Navigation, Monterey, California, 18-20 January 2006; pp. 564-573.

[19] Gelb, A., "Applied Optimal Estimation," the MIT Press, 2001. ISBN: 0-262-57048-3

[20] AIAA, Education Series, J.S. Przemieniecki/series editor-in-chief. An introduction to the Mathematics and Methods of Astrodynamics, Revised Edition. Richard H. Battin

[21] J. Rife, S. Pullen, P. Enge, and B. Pervan, "Paired Overbounding for Nonideal LAAS and WAAS Error Distributions," IEEE Transactions on Aerospace and Electronic Systems, Vol. 42, No. 4, October 2006, pp. 1386-1395.